Environ. Water Eng., 2025, 11(4), 438-449 https://doi.org/10.22034/ewe.2025.522302.2020

EWE

Environment and Water Engineering

Homepage: www.jewe.ir

ISSN: 2476-3683

Adsorption of red hair dye from aqueous solution using Fe_3O_4@NH_2-SBA-16 NCs: Equilibrium, kinetic, and thermodynamic studies

Hassan Neysi[1], Farzaneh Marahel[1]✉, Alireza Geramizadegan[2], and Sadifollah Shirvan[1]

[1]Department of Chemistry, Omidiyeh Branch, Islamic Azad University, Omidiyeh, Iran
[2]Department of Chemistry, Dashtestan Branch, Islamic Azad University, Dashtestan, Iran

ARTICLE INFO

Paper Type: Research Paper

Received: 09 May 2025
Revised: 29 May 2025
Accepted: 02 June 2025
Published: 08 July 2025

Keywords
Adsorption
Cycles
Magnetic Nano-Adsorbent
Red Hair Dye

Corresponding author:
F. Marahel
✉ f.marahel@iau.ac.ir

ABSTRACT

This study investigated the potential of Fe3O4@NH2-SBA-16 nanocomposites (NCs) for adsorbing red hair dye from aqueous solutions. The nanocomposite was thoroughly characterized using BET, FT-IR, XRD, SEM, and TGA, confirming its structural integrity and functional groups. The adsorption behavior of Fe3O4@NH2-SBA-16 NCs was tested by changing several parameters such as pH, dye concentration, adsorbent amount, thermodynamics, and contact time. The maximum adsorption capacity for red hair dye on Fe3O4@NH2-SBA-16 NCs was 16.1 mg/g at 25 °C. Kinetic studies indicated that dye removal follows pseudo-second-order kinetics. Thermodynamic parameters, including ΔG°, ΔH°, and ΔS°, were calculated as -3.66 kJ/mol, -16.08 kJ/mol, and -40.92 J/mol·K, respectively. Results showed the adsorption process to be exothermic and spontaneous based on these thermodynamic parameters. In real water samples, removal efficiency reached 96.8%, although it decreased to 90.5% with increasing salt concentration. The magnetic nano-adsorbent also demonstrated excellent reusability over three cycles. Overall, the findings suggest that Fe3O4@NH2-SBA-16 NCs are a promising, eco-friendly adsorbent for removing red hair dye from aqueous solutions.

Highlights

- Findings highlight Fe_3O_4@NH_2-SBA-16NCs is an Eco-friendly adsorbent for red hair dye removal,
- In real water samples, the significantly red hair dye removal efficiency reached 96.8%,%,
- Adsorbent has a superb three-cycle by a slight decrease of 2.05% usage capacity,

Citing:
Neysi, H., Marahel, F., Geramizadegan, A., & Shirvan, S.(2025). Adsorption of red hair dye from aqueous solution using Fe_3O_4@NH_2-SBA-16 NCs: Equilibrium, kinetic, and thermodynamic studies. *Environment and Water Engineering*, *11*(4), 438-449. https://doi.org/10.22034/ewe.2025.522302.2020

1. Introduction

One of the biggest issues in today's world is undoubtedly environmental pollution. As a result of increasing industrial, agricultural, and urban activities of human beings, disregarding nature, large amounts of pollutants have been released into the natural environment. One of the most prominent of these pollutants is synthetic dyes. Synthetic dyes come in a wide variety and are produced in incredible quantities to meet increasing demand. Unfortunately, a significant amount of synthetic dyes is released into the aquatic environment during the production and usage processes. These synthetic pollutants are substances that are not or have very difficult to biodegradable and can accumulate. They also have very harmful effects on organisms, such as mutagenic, carcinogenic, and even teratogenic activities (Gupta et al., 2013; Li et al., 2014; Corrêa et al., 2020). Due to these properties, synthetic dyes cause numerous biological activity problems and even deaths in all biota, starting with living creatures in aquatic ecosystems. As a result of their potential toxicity, carcinogenicity, and mutagenicity, these waste products are a serious threat to human health (Mohamadia et al., 2023).

Many dyes are carcinogenic, toxic, and mutagenic to both humans and animals due to the presence of aromatic rings in their structure (Kaith et al., 2019; Sorour et al., 2024). Thus, it is necessary to remove these dyes from wastewater before its final disposal. Due to its extended environmental persistence and prolonged shelf life, hair dyes are a recalcitrant dye

molecule, and exposure may cause irritation, redness, and swelling at the site of contact. The adverse effects of hair dye exposure include permanent skin discoloration, allergic reactions, dermatitis, and necrosis (Al-Ma'abreh et al., 2022; Kosale et al., 2023).

Red hair dye is a basic hair dye. It is a semi-permanent or temporary hair dye. This product appears as a red powder, and it is used in gel, cream, shampoo, mousse, and lotion applications (Al-Ma'abreh et al., 2022; Sorour et al., 2024). The hair dyes in the fashion industry in the sewage system can harm the environment. The contamination of artificial dyes into water streams without pre-treatment causes excessive health risks to aquatic organisms by increasing chemical oxygen demand and results in carcinogenic, mutagenic, and allergic effects on human beings. Adsorption using ion exchangers is one of the best methods for the removal of dyes from wastewater (Sobhanardakani et al., 2017; Al-Ma'abreh et al., 2022).

Aromatic-based molecular dyes that come from hydrocarbons such as benzene, toluene, etc., have specific environmental risks. Several methods have been used to remove toxic compounds, including membrane filtration, ion exchange, precipitation, coagulation-flocculation, ozonation, biosorption, and photodegradation (Ghosh and Sinha, 2008; Zahir et al., 2014; Ahmad et al., 2015; Souza et al., 2020). However, these methods have some limitations, such as high costs, the generation of secondary waste that is difficult to handle, prolonged processing times, and limited reusability. Adsorption has emerged as a preferred method to remove dyes because of its ease of application, cost-effectiveness, simplicity, versatility, and environmental sustainability (Yang et al., 2015; Radha et al., 2023). Initially, these adsorbents were of interest due to their high adsorption capacity and availability, but the drawbacks of these adsorbents have led to a focus on a different family of adsorbents.

Mesoporous materials, as a subset of nanomaterials with nano-sized pores and a very high internal surface area, have a high capability for adsorption and interaction with atoms, molecules, and ions. Among silicate mesoporous materials with structured order and narrow pore distribution, categories like m-SiO_2, MCM41, and n-SBA can be mentioned (Kiomarsipour et al., 2021; Davoudi, 2022; Abidin et al., 2022). An important and non-toxic group of these mesoporous materials is the SBA family (Wang et al., 2018). SBA-type mesoporous materials belong to the ceramic family and were first synthesized in 1998. Among the mesoporous SBA compounds, SBA-16 is a three-dimensional cubic cage (Zhao et al., 1998). Mesoporous nanomaterials, such as SBA-16 (mobile composition of material no. 16), are suited for use as nanoparticle additives because they have large specific surface areas. SBA-16 facilitates higher mass transfer due to its highly effective surface area and interconnected three-dimensional channels (Feliczak-Guzik et al., 2016; Anyat et al., 2025; Zolfaghari and Zanganeh Assadabadi, 2025). SBA-16 causes higher mass transfer due to its highly effective surface area and connected three-dimensional channels. In the synthesis process of this porous mesopore, non-ionic surfactants are often used. Also, the active sites of SBA-16, adding a variety of ligands (organic groups, coordination compounds, nanoparticles, metal oxides, etc.) and loading different compounds onto them, have a highly effective capability for adsorption of materials (Emrani et al., 2023; Anyat et al., 2025; Zolfaghari and Zanganeh Assadabadi, 2025).

In recent years, the dyes in the fashion industry in the sewage system can hurt the environment. However, wastewater from the fashion industry will be more to handle. Among modern treatment technologies, adsorption is an effective treatment. Notably, this study marks the utilization of Fe_3O_4 nanoparticles in the modification of SBA-16/NH_2 to augment its adsorptive properties. This innovative combination serves as a novel platform for enhanced adsorption capabilities, particularly in the removal of dyes from water and wastewater. Also, the relatively high saturation magnetization values of Fe_3O_4@NH_2-SBA-16NCs make it susceptible to magnetic fields and easy to separate from aqueous solutions. Because the absence of significant hysteresis and remanence in Fe_3O_4@NH_2-SBA-16NCs is crucial for adsorption and removal materials. In this ecological-focused article aimed at eliminating harmful substances from the environment, we investigated the potential of Fe_3O_4@NH_2-SBA-16NCs for the removal of red hair dye from aqueous solutions using the adsorption method.

This study focuses on the preparation of Fe_3O_4@NH_2-SBA-16NCs and its application for the removal of red hair dye. Also, equilibrium adsorption processes are investigated and isotherm, kinetic models and examining successive cycles of adsorption-desorption are evaluated to better understand the adsorption behavior.

2. Materials and Methods

2.1 Reagents and chemicals

The reagents utilized for this work were purchased from Sigma-Aldrich Chemical Company (USA), and they are of analytical grade. Red hair dye (2-Naphthalenaminium, 7-hydroxy-8-[(2-methoxyphenyl) azo] - N, N, N- trimethyl - chloride (68391-30-0, MW of 371.86 g/mol), 98%), Pluronic F127 copolymer, 3-aminopropyltriethoxysilane (APTES), Tetraethyl orthosilicate (TEOS), Ferric chloride hexahydrate ($FeCl_3 \cdot 6H_2O$, 99%), Ferrous chloride tetrahydrate ($FeCl_2 \cdot 4H_2O$, 98%), Ammonium hydroxide (NH_4OH, 98%), and Ethanol (98%). All solutions were prepared using double-distilled water. pH adjustments were performed using 0.1 mol/l hydrochloric acid (HCl) or 0.1 mol/l sodium hydroxide (NaOH), as required. Three stock solutions of 1000 mg/l concentrations were prepared by dissolving 1.0 g of red hair dye in distilled water.

2.2 Apparatus

FTIR spectra were obtained using a PerkinElmer FTIR spectrometer (400–4000 cm^{-1}). PXRD analysis was done by Bruker D8 Advanced X-ray diffractometer (2θ = 5–70°) with Cu Kα radiation (λ = 1.5418 Å). FESEM images were obtained using JEOL JSM 6610LV. BET-BJH analysis for specific surface area and pore size distribution was done using a Quanta Chrome Nova Win at 77 K. UV–vis absorption spectra were used to record dye concentration at λ_{max} = 518 nm at room temperature using a Shimadzu UV–Vis 1900i

spectrophotometer. Solution pH was maintained using Eutech Scientific Thermo Fischer.

2.3 Synthesis of Fe_3O_4 nanoparticles

Fe_3O_4 NPs were prepared according to a previously reported method. First, 0.86 g of $FeCl_2{\cdot}4H_2O$, 2.35 g $FeCl_3{\cdot}6H_2O$ (molar ratio of Fe^{2+}: Fe^{3+}=1:2) were dissolved in 10 ml of distilled water, respectively. They were dissolved in 40 ml of deoxygenated water with vigorous stirring at a speed of 500 rpm. Then, 10 ml of 28% NH_4OH was added to the flask under stirring (pH~9). The reaction was continued for 1 h at 90 °C under constant stirring and a nitrogen environment. Indeed, the N_2 (g) bubbling through the mixture protects Fe_3O_4 against the critical oxidation. Then, the sample was stirred in a three-hole beaker under a nitrogen atmosphere. The precipitate obtained (black color) was separated from the solvent by a magnet and washed with 98% ethanol. After completion of the reaction, the autoclave is gradually cooled to room temperature. The magnetite (Fe_3O_4) nanoparticles are then separated from the solution using a magnet and washed three times with deionized water and ethanol. Finally, the nanoparticles are vacuum-dried at 60 °C for 12 hr.

2.4 Synthesis of SBA-16-NH_2

To enhance the adsorption efficiency of SBA-16, it was functionalized with amino (-NH_2) groups. For the synthesis, 2.0 g of Pluronic F127 copolymer was dissolved in 150 ml of distilled water and 15 mL of hydrochloric acid (HCl). The solution was stirred for 30 minutes, after which 15 ml of 1-butanol was added and stirring was continued for an additional 1 hour. Subsequently, predetermined amounts of tetraethyl orthosilicate (TEOS) and 3-aminopropyltriethoxysilane (APTES) were introduced into the mixture under continuous stirring. The reaction mixture was then stirred at 40 °C for 8 hours, followed by hydrothermal treatment at 120 °C for 12 hours in an oven. Finally, the template (Pluronic F127) was removed via ethanol extraction, yielding the functionalized SBA-16-NH_2 material.

2.5 Synthesis of Fe_3O_4@NH_2-SBA-16NCs

The Fe_3O_4@NH_2-SBA-16 nanocomposites were synthesized via a suspension cross-linking process. We used an ultrasonic bath in the solution. In a typical procedure, 0.05 g of Fe_3O_4 nanoparticles was dispersed into a solution containing 0.2 g of SBA-16-NH_2, and the mixture was stirred continuously at 60 °C for 5 hours under N_2 gas to ensure uniform interaction between the components. The resultant product was washed with ethanol, filtered, and dried overnight at 60 °C in an oven. The permanent magnet was used to separate the resulting nanocomposites from the suspension. The collected Fe_3O_4@NH_2-SBA-16 NCs were then washed with ethanol to remove unbound residues and dried under vacuum at 50 °C or 80 °C for 2 hours.

2.6 Preparation of red hair dye sample

Red hair dye was provided by a local medical company in Ahvaz city, Iran. The desired red hair dye concentration was obtained by diluting the stock red hair dye solution (1000 mg/l). A standard curve was created by measuring the absorbance of red hair dye (618 nm) using a spectrophotometer (Shimadzu UV–Vis 1900i) to determine red hair dye concentration in samples.

2.7 Batch analysis

To illustrate the adsorption efficiency, the batch study of Fe_3O_4@NH_2-SBA-16 NCs was carried out at 25 °C. To perform the contact time study, 0.2 g of Fe_3O_4@NH_2-SBA-16 NCs was dissolved in 100 ml of red hair dye of concentration 10 (mg/l). The optimization of red hair dye adsorption using Fe_3O_4@NH_2-SBA-16 NCs examined the effects of parameters affecting red hair dye removal, including initial dye concentration, pH, and dosage adsorbent in the range of 0.02 to 2.0 g, were studied. Time intervals from 10 to 80 min were agitated at a constant rate of 180 rpm in a temperature-controlled orbital shaker maintained at 25 °C. After a fixed interval of 65 min, 3 ml of the sample was taken out, and red hair dye concentration was recorded using a Shimadzu UV–vis spectrophotometer at λ_{max} = 518 nm. To calculate maximum equilibrium adsorption capacity (qe), and adsorption percentages (% R), using Eqs. 1 and 2 (Al-Ma'abreh et al., 2022; Biuki et al., 2025).

$$qe = \frac{V(C_0 - C_e)}{M} \times 100 \quad (1)$$

$$R\% = \frac{C_0 - C_e}{C_0} \times 100 \quad (2)$$

where C_0 (mg/l) is the Initial red hair dye concentration, C_e (mg/l) is final red hair dye concentration, M (g) is amount of the Fe_3O_4@NH_2-SBA-16NCs, and V (l) is volume of the solution.

3. Results and discussion

3.1 Characterization

3.1.1 BET analysis

The BET surface area, average pore diameter, and the BJH curve in the range of 1-100 nm are seen in Fig. 1a. Using this curve, the distribution of holes can be measured. As can be seen, the maximum distribution of holes is in the range of ~2-50 nm. Also, the BET results of Fe_3O_4@NH_2-SBA-16 NCs indicate that the specific surface area of Fe_3O_4@NH_2-SBA-16 NCs is 19.158 m^2/g. Also, the average particle diameter and pore volume are 17.894 nm and 0.086 cm^3/g, respectively, as summarized in (Fig. 1). The adsorption capacity of Fe_3O_4@NH_2-SBA-16NCs is strongly influenced by their porosity and the chemical reactivity of surface functional groups. The adsorption capacity increases with an increase in the number of adsorbed Fe_3O_4 nanoparticles, and the relative partial pressure range on the adsorption isotherms gradually decreases. This is because the Fe_3O_4 nanoparticles, in the composite, spread into SBA-16/NH_2 channels, making the channels narrow and the pore volume decreased. The gradual decrease of the BET specific surface area indicates that the Fe_3O_4 nanoparticles were introduced into the SBA-16/NH_2 channels, the most probable pore diameter reduced, indicating that the Fe_3O_4 nanoparticles entered the SBA-16/NH_2 channels.

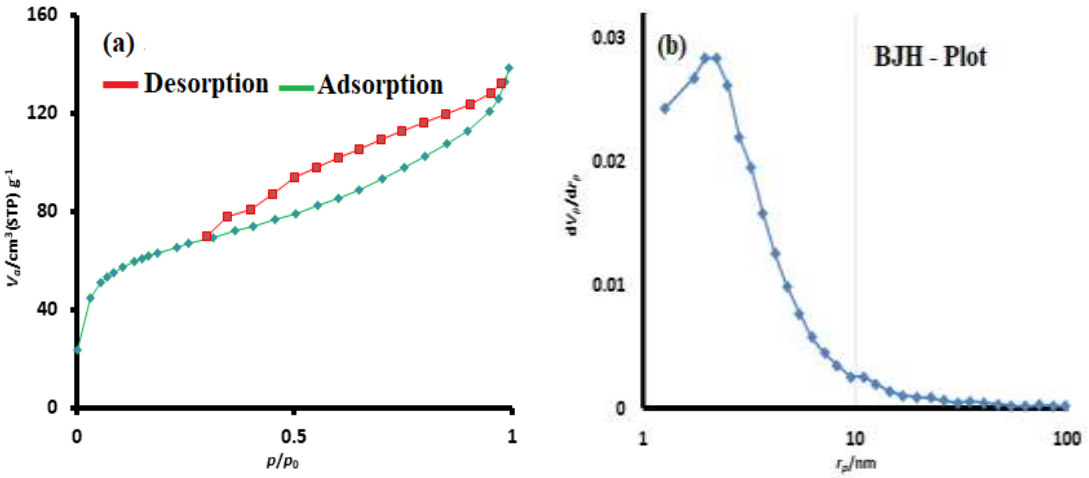

Fig. 1: a) N_2 adsorption–desorption isotherms, b) Pore size distributions of Fe_3O_4@NH_2-SBA-16 NCs

3.1.2 FT-IR, XRD, and SEM images of Fe_3O_4@NH_2-SBA-16 NCs

The FT-IR spectrum of Fe_3O_4@NH_2-SBA-16 NCs (Fig. 2a) displays a broad absorption band around 3510 cm^{-1}, attributed to –OH groups from silanol (Si–OH) and adsorbed water molecules on the silica surface. Characteristic peaks observed at 3441.12 cm^{-1} and 1630.95 cm^{-1} correspond to the stretching and bending vibrations of the silanol groups in SBA-16/NH_2 and Fe_3O_4@NH_2-SBA-16NCs (Feliczak-Guzik et al., 2016; Zolfaghari and Zanganeh Assadabadi, 2025). In addition, distinct bands at 1086.21 cm^{-1}, 949.10 cm^{-1}, and 797.37 cm^{-1} are assigned to the asymmetric and symmetric stretching vibrations of Si–O–Si bonds, confirming the integrity of the mesoporous silica framework. A sharp absorption peak at 862.66 cm^{-1} corresponds to Fe–O stretching, confirming the presence of Fe_3O_4 nanoparticles in the nanocomposite (Wang et al., 2018). The XRD pattern of Fe_3O_4@NH_2-SBA-16NCs is shown in Fig. 2b. is composed of distinct peaks at 2θ =30.1, 35.6, 39.2, 44.4, 54.2, and 63.1 belong to reflections from the (220), (311), (400), (422), (511), and (440) which, accordingly approved and has good agreement with standard JCPDS data (Feliczak-Guzik et al., 2016; Anyat et al., 2025). These results confirm the successful incorporation of magnetite nanoparticles into the SBA-16 framework. SEM micrographs presented in Figs. 2c, 2d, and 2e reveal the surface morphology, particle size, and shape of SBA-16/NH_2, Fe_3O_4@NH_2-SBA-16NCs, and pure Fe_3O_4 nanoparticles, respectively. As depicted in SEM micrographs, the various sizes, in the range of 2-50 nm, are very close to those determined by XRD analysis.

3.1.3 TGA analysis for Fe_3O_4@NH_2-SBA-16NCs

Thermal gravimetric analysis (TGA) of Fe_3O_4@NH_2-SBA-16NCs was done to study the thermal stability of samples (Fig. 3a). The mass loss at ~10-100 °C corresponds to the release of absorbed moisture. At higher temperatures, decomposition of the amine group began and was completed at 800 °C. At 350 °C, we observed a single main peak in samples modified with amine groups (Fig. 3a).

3.1.4 Determination Point-of-Zero Charge (pHpzc)

To determine the point of zero charge (PZC), i.e., the pH at which there is zero electric charge on the surface of synthesized Fe_3O_4@NH_2-SBA-16NCs, 50 ml of 0.01 M NaCl solution was added in 100 mL Erlenmeyer flasks, and pH was adjusted from 1 to 9 using 0.01 M NaOH. 0.1 g of the Fe_3O_4@NH_2-SBA-16NCs was added to the flasks, and the solutions were agitated at 180 rpm for 24 h at 25 °C using a laboratory rotatory shaker. The supernatant was decanted, and its pH_f was measured. The PZC was determined from the graphical plot of pH_i vs. ΔpH (pH_i-pH_f), and pH of 7.0, the surface of Fe_3O_4@NH_2-SBA-16NCs has a point of zero charge (PZC) (Fig. 3b). As shown in Fig. 3b, the difference between the initial and final pH values (pH_{PZC} - pH_i) was plotted against the pH (Feliczak-Guzik et al., 2016; Einolghozati et al., 2022).

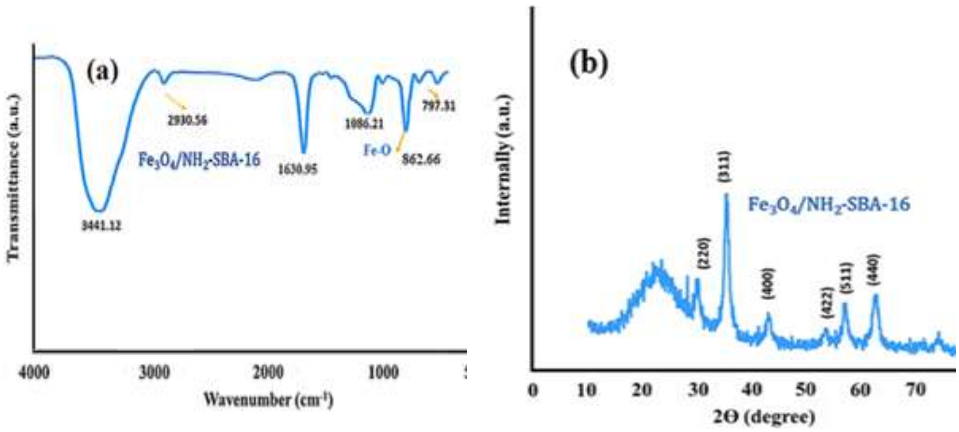

Fig. 2: a) FT-IR spectrum of Fe_3O_4@NH_2-SBA-16NCs, (b) XRD patterns of Fe_3O_4@NH_2-SBA-16 NCs, and SEM micrograph of c) SBA-16/NH_2, d) Fe_3O_4@NH_2-SBA-16 NCs, and e) Fe_3O_4 NPs.

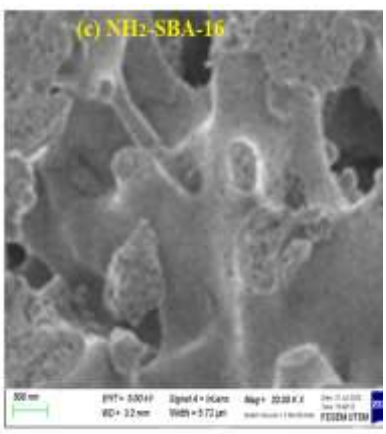

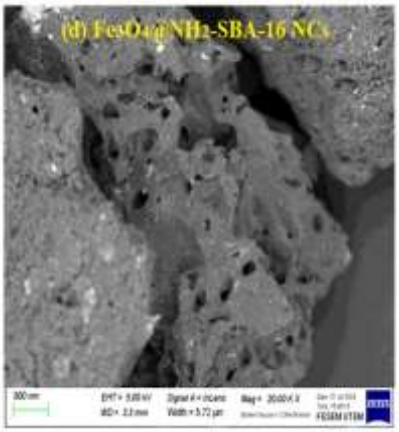

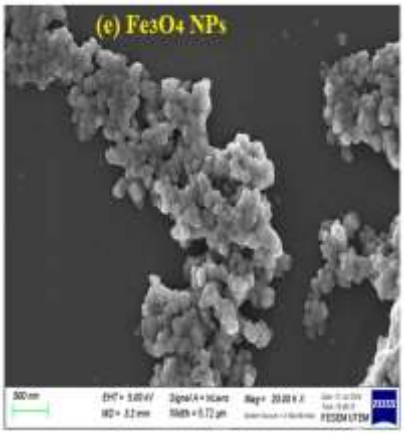

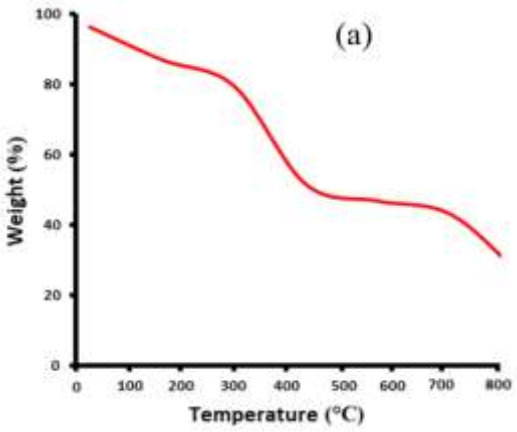

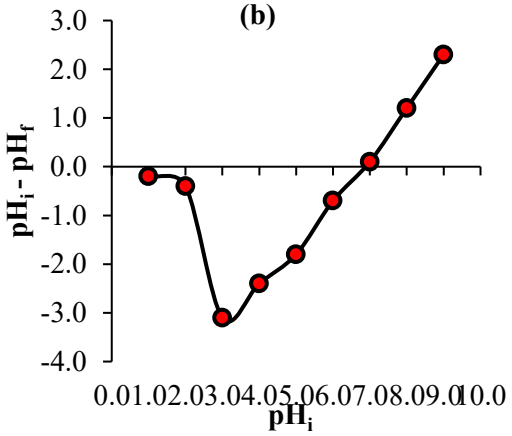

Fig. 3: a) TGA, and b) pHpzc on the adsorption of Fe_3O_4@NH_2-SBA-16 NCs

3.2 Optimized parameters

3.2.1 Impact of pH

Impact of pH on red hair dye adsorption by Fe_3O_4@NH_2-SBA-16NCs was examined in the range of pH 2-8. Fig. 4a displays the pH effect on red hair dye purification. The effect of pH on red hair dye reduction via the adsorption process at acidic pH is better than the higher and alkaline pH. According to the suggested value of pHZPC (i.e., the high efficiency of red hair dye reducing in acidic pH, especially pH = 6.5) occurs due to electrostatic attraction among negative charge molecules of adsorbent and compounds related to red hair dye, leading to the clean up of wastewater. The positive charge surface should be absorbent (pH<pHZPC), while at higher pH the adsorbent surface has a negative charge so and accordingly, as a consequence of the electrostatic repulsion force between the negative charge ions of the adsorbent surface, hinders their subsequent adsorption, which subsequently leads to a reduction in red hair dye of wastewater. However, the abatement in red hair dye removal at pH <6.5 occurred due to the competition of red hair dye with H^+. Additionally, in highly acidic pH, the sharp concentration of H^+ sets the scene for the protonation of atoms on the surface of adsorbents and provokes the reduction of interaction with red hair dye and the surface of adsorbents. Both reasons, precipitation of hydroxide and conversion of red hair dye, provoked the reduction in red hair dye removal at pH >6.5. This phenomenon obstructed the access of red hair dye to adsorption sites and culminated in less adsorption of red hair dye on Fe_3O_4@NH_2-SBA-16NCs (Sobhanardakani et al. 2017; Davoudi, 2022).

3.2.2 Impact of the dosage of Fe_3O_4@NH_2-SBA-16NCs adsorbent

The effect of varying the initial adsorbent dosage on removal efficiency was analyzed within the range of 0.02 to 2.0 g. As shown in Fig. 4b, the adsorbent dosage has a positive effect on the removal efficiency, and maximum removal was attained at the initial Fe_3O_4@NH_2-SBA-16 NCs dosage of 0.2 g. Increasing the dosage of Fe_3O_4@NH_2-SBA-16 NCs enhances the removal efficiency of red hair dye, primarily due to the expanded surface area and the greater availability of adsorption sites (Jamshidi et al., 2022). The increase in removal efficiency is due to higher surface area and availability of more specified sites concerned with Fe_3O_4@NH_2-SBA-16 NCs surface for the target molecules, leading to improvement in method efficiency (raising the number of available adsorption sites). After optimal conditions owing to the instauration of adsorption sites during waste wastewater treatment process or overlapping and conglomeration of active sites at a higher dosage, the rate of adsorption enhancement becomes slow or does not affect significantly (Davoudi, 2022).

3.2.3 Impact of time on the adsorption

The contact time plays a significant role in determining the removal percentage. The impact of contact time on the adsorption of red hair dye using Fe_3O_4@NH_2-SBA-16NCs

adsorbent was defined at different contact times (10-80 min) for red hair dye while keeping another parameter constant. A considerable increase in the red hair dye was observed for the contact time of 65 min. Fig. 4c shows the effect of contact time on the adsorption for adsorption red hair dye by Fe_3O_4@NH_2-SBA-16N Cs. Based on this figure, the optimum contact time may be chosen as 65 min (Dehvari et al., 2017; Marahel et al., 2023).

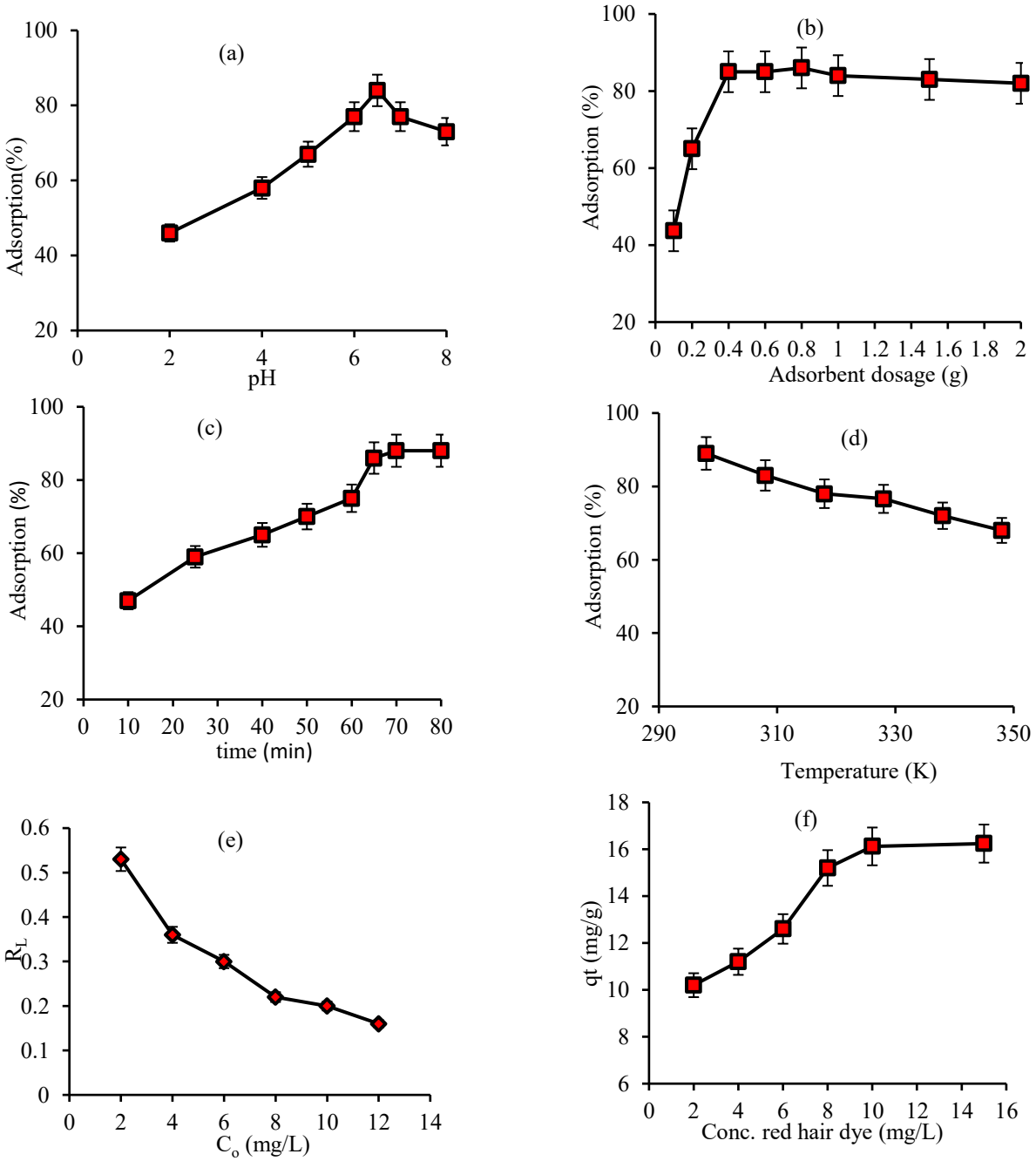

Fig. 4: a) Impact of pH (dosage adsorbent = 0.2 g, t = 65 min), b) Impact of dosage of adsorbent (pH =6.5, t = 65 min), c) Impact of time (pH =6.5, dosage adsorbent = 0.2 g), d) Impact of temperature for red hair dye adsorption on Fe_3O_4@NH_2-SBA-16NCs adsorbent (pH = 6.5, dosage adsorbent = 0.2 g, t = 65 min), e) Impact of isotherm (R_L) (pH = 6.5, dosage adsorbent = 0.2 g, t = 65 min), f) Impact of equilibrium (pH = 6.5, dosage adsorbent = 0.2 g, t = 65 min)

3.2.4 Impact of temperature

To study the impacts of temperature on the adsorption of red hair dye on Fe_3O_4@NH_2-SBA-16 NCs, the experiments were performed at temperatures from 298 to 348 K. (Fig. 4d) shows the influence of temperature on to removal of red hair dye on Fe_3O_4@NH_2-SBA-16NCs. As can be seen, the adsorption of red hair dye on Fe_3O_4@NH_2-SBA-16NCs in the process decreases with increasing temperature. This may come from the fact that the adsorption process may be an exothermic one (Qin et al., 2014; Dehvari et al., 2017).

3.3 Equilibrium isotherms

The adsorption isotherm explains the relationship between the quantity of adsorbed substance and the residual concentration of dye in the solution. It shows the distribution of adsorbed molecules between the liquid and the solid. Equilibrium

isotherms are very important in designing any adsorption process. Fig. 4e and f indicate the adsorption isotherms of red hair dye on the surface of Fe_3O_4@NH_2-SBA-16 NCs, respectively. The adsorption capacity (at 25 °C) is around 16.1 mg/g for red hair dye on the surface of Fe_3O_4@NH_2-SBA-16NCs, respectively (Pournamdari and Niknam 2024; Ahmeet al., 2024).

3.4 Adsorption study

The retention capacities of pollutants and the maximum adsorption mechanisms are evaluated using adsorption isotherms. The relationship between the dye molecules adsorbed on the Fe_3O_4@NH_2-SBA-16NCs surface, and the dye molecules remaining in the solution was investigated using widely used isotherm models such as Langmuir, Freundlich, and Temkin isotherms (EL–Desouky and EL-Bindary, 2021; Ahmeet al., 2024). The Langmuir, Freundlich, and Temkin isotherms were estimated using Eqs. 3, 4, and 5, respectively.

$$q_e = \frac{q_m K_L C_e}{1+K_L C_e} \quad R_L = \frac{1}{1+K_L C_0} \qquad \text{Langmuir} \qquad (3)$$

$$q_e = q_m K'_F + C_e^{\frac{1}{n}} \qquad \text{Freundlich} \qquad (4)$$

$$q_e = q_m (B'_T \ln A_T C_e) \qquad \text{Temkin} \qquad (5)$$

where C_e is the red hair dye equilibrium concentration of the solution (mg/l), q_m represents the maximum value of q_e, which is necessary for the monolayer covering the whole surface of the used adsorbent. $q_m K'_F = K_F$, the Freundlich model, K_F is the Freundlich constant that indicates adsorption capacity (mg/g). Also, $q_m B'_T = B_T$, the Temkin model, A_T and B_T are the Temkin constants determined experimentally. The chi-square (X^2) tests were adopted to determine the suitability of the isotherm model to the experimental data (Pournamdari et al., 2024). The X^2 equation is as follows:

$$X^2 = \sum \frac{(q_e - q_{e.m})^2}{q_{e.m}} \qquad (6)$$

where q_e (mg/g) is the experimental equilibrium capacity and q_e, m (mg/g) is the equilibrium capacity obtained from the model.

The adsorption process for red hair dye on the surface of Fe_3O_4@NH_2-SBA-16NCs is best described by the Langmuir isotherm model, with a maximum adsorption capacity of 16.1 mg/g and a high degree of correlation (R^2 = 0.994). This indicates monolayer adsorption on homogeneous adsorption sites with moderate adsorbent-adsorbate interaction. The Langmuir model proved to be the most accurate for describing the red hair dye- Fe_3O_4@NH_2-SBA-16NCs adsorption system, exhibiting the lowest error. The Freundlich and Temkin model, while secondary, highlights some heterogeneity in the adsorption sites but is less significant in describing the overall process shown in Table 1 (EL–Desouky and EL-Bindary, 2021).

3.5 Adsorption kinetic equation

The adsorption kinetics of red hair dye by Fe_3O_4@NH_2-SBA-16NCs was followed by applying the pseudo-first-order, pseudo-second-order, and Elovich models, which can be described by the differential forms represented in Eqs. 7, 8, and 9, respectively (EL–Desouky and EL-Bindary, 2021).

Table 1 The adsorption isotherm of red hair dye on the Fe_3O_4@NH_2-SBA-16 NCs (pH = 6.5, dosage sorbent = 0.2 g, t = 65 min)

Isotherm	Parameters	R% red hair dye
Langmuir	q_m (mg/g)	16.1
	K_L (L/ mg)	1.03
	R^2	0.994
	X^2	0.96
Freundlich	1/n	0.31
	K_F (mg)$^{1-n}$ $L^n g^{-1}$	15.2
	R^2	0.881
	X^2	1.37
Temkin	A_T (l/ mg)	1.1
	B_T	10.5
	R^2	0.617
	X^2	1.72

$$\ln(q_e - q_t) = \ln q_e - K_i\, t \qquad (7)$$

where q_e and q_t are respectively the quantities of solute adsorbed in mg/g at equilibrium and at time t and k_1 is the first order rate constant (1/min) (Al-Ma'abreh et al., 2022; Biuki et al., 2025).

$$\frac{t}{q_t} = \frac{1}{K_2 q_e^2} + \frac{t}{q_e} \qquad (8)$$

k_2 is the second-order rate constant (mg/g. min) (Pournamdari and Niknam, 2024). The Elovich isotherm is based on the principle of kinetics, assuming that the number of adsorption sites increases exponentially with adsorption, thus implying multilayer adsorption described by the following equation:

$$q_t = \frac{1}{\beta} \mathrm{Ln}\alpha\beta + \frac{1}{\beta} \mathrm{Ln}t \qquad (9)$$

The adsorption capacity at equilibrium, α is (mg/g. min), and β is the adsorption constant (g/mg). To assess the adsorption kinetics of red hair dye on the Fe_3O_4@NH_2-SBA-16NCs adsorbent, six samples were created, with each sample comprising 100 ml of dye solution at a concentration of 10 mg/l.

Table 2 The first-order, second-order model, and Elovich model reactions parameters of red hair dye on the surface of Fe_3O_4@NH_2-SBA-16NCs (pH = 6.5, dosage adsorbent = 0.2 g, t = 65 min)

Models	parameters	R% red hair dye
First-order model kinetic	k_1(1/min)	0.065
	q_e (mg/g)	14.2
	R^2	0.958
Second-order model kinetic	k_2 (1/min)	0.053
	q_e (mg/g)	16.1
	R^2	0.997
Elovich	α (mg/g. min)	6.43
	β (g/mg)	0.3
	R^2	0.899

An adsorbent dosage of 0.2 g was then added to each sample. Then, at times of 5, 20, 35, 50, 65, and 80 minutes and at the

optimal pH of 6.5, the samples were investigated to the usual kinetic models, including pseudo-first order, pseudo-second order, and Elovich (Ahmad et al., 2024; Einolghozati et al., 2022). The pseudo-second-order kinetic model appears to be the most appropriate for describing dye adsorption on the Fe_3O_4@NH_2-SBA-16NCs adsorbent. Earlier studies have confirmed the effectiveness of this model in removing hair dyes from aqueous solutions. The results are shown in Table 2.

3.6 Thermodynamic study

Thermodynamic parameters such as Gibbs free energy change (ΔG°), enthalpy change (ΔH°), and entropy change (ΔS°) were calculated using the thermodynamic data and Eqs. 10, and 11. (Davoudi, 2022).

$$\ln K_{ad} = \frac{\Delta S^{\circ}_{ad}}{R} - \frac{\Delta H^{\circ}_{ad}}{RT} \quad (10)$$

$$\Delta G^{\circ}_{ad} = \Delta H - T\Delta S \quad (11)$$

Where K_{ad} is the Langmuir constant, T is the temperature in Kelvin, and R is the universal gas constant (8.314 J/molK). ΔH° and ΔS° values were obtained from the slope and intercept of the lnK_{ad} vs. 1/T plot (El Haddad 2016; Pournamdari et al., 2024). Table 3 presents a summary of the calculated thermodynamic parameters. The negative ΔG° value is a strong indicator of a spontaneous and thermodynamically favorable adsorption process. The negative ΔH° values strongly indicate that the adsorption process is exothermic. The negative ΔS° in adsorption indicates the in decrease of disorder in the solid-solution surface during the adsorption process and the creation of some structural changes in the adsorbent and the adsorbed, and as a result, the adsorption process is reversible. The ΔH° value of -16.08 kJ/mol further supports the physisorption nature of the adsorption process. The adsorption mechanism of red hair dye onto the developed Fe_3O_4@NH_2-SBA-16NCs adsorbent involves a combination of hydrophobic interactions, hydrogen bonding, and electrostatic forces, driven by the amphiphilic nature of the functionalized silica-coated magnetic nanoparticles. The second major interaction between the adsorbate molecules and the adsorbent is hydrogen bonding.

Table 3 The thermodynamic parameters for the adsorption of the dye (pH = 6.5, dosage of adsorbent = 0.2 g, t = 65 min)

Hair dye	T (^{O}K)	value of ΔG° (kJ/mol)	value of ΔH° (kJ/mol)	value of ΔS° (J/mol. K)
(Red hair dye =10 (mg/l)	288	-3.66	-16.08	-40.92
	308	-3.79		
	318	-3.52		
	328	-3.17		
	338	-2.14		
	348	-1.61		

The unmodified –OH groups on the silica surface form hydrogen bonds with the ester carbonyl (–C=O) groups of red hair dye. Similarly, the APTES-derived amine groups (NH_2) can act as hydrogen bond donors/acceptors with dye oxygen atoms (El Haddad 2016; Anyat et al., 2025). Additionally, intermolecular interactions rather than chemical bonding. The adsorption mechanism involves multiple forces, with electrostatic interactions playing a key role by attracting the cationic red hair dye to negatively charged sites on the Fe_3O_4@NH_2-SBA-16NCs surfaces.

3.7 Binary mixture of dyes

To check the potential of synthesized adsorbent in the dye removal efficacy of more complex systems, red hair, yellow hair, and blue hair dyes were added into the aqueous solution by maintaining the 1:1 ratio with a concentration of 10 mg/l of both dyes and 0.2 g adsorbent was added into it and subjected for shaking in an orbital shaker for 65 min at ambient temperature. For the binary system, absorption maxima of red hair, yellow hair, and blue hair dyes were recorded at 518 nm, 553 nm, and 637 nm. It was observed that Fe_3O_4@NH_2-SBA-16NCs has good removal efficiency towards red hair dye, yellow hair dye, and blue hair dye in binary systems, and the maximum adsorption efficiency red hair dye (91 %) yellow hair dye (86 %), and blue hair dye (81 %), respectively. This may be attributed to the fact that adsorption occurs with molecules that are small enough in size to enter the inner cavities and diffuse through the pores with the least steric hindrance especially in the micropore region for these small molecules. The molecules yellow hair dye and blue hair dye have molecular diameters greater than molecular red hair dye. Therefore, the maximum adsorption capacity, maximum adsorption efficiency and adsorption rate increase with decreasing size of the adsorbed molecules. The results are shown in (Fig. 5).

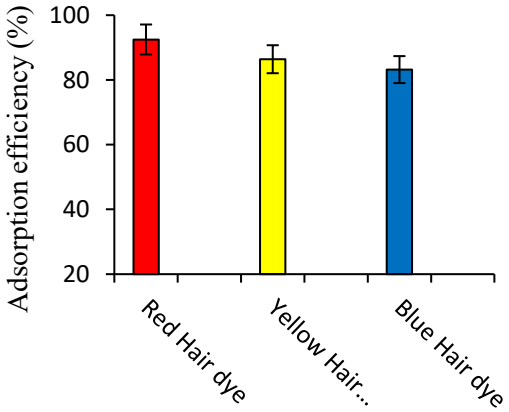

Fig. 5 Plot of adsorption efficiency simultaneous removal of red hair, yellow hair, and blue hair dyes on the surface of Fe_3O_4@NH_2-SBA-16 NCs (pH = 6.5, dosage adsorbent = 0.2 g, t = 65 min).

3.8 Effect of ionic strength

The effect of ionic strength on the adsorption of red hair dye using Fe_3O_4@NH_2-SBA-16NCs adsorbent, with sodium chloride (NaCl) as the ionic strength agent. NaCl was prepared in five distinct concentrations: 0.1, 0.2, 0.5, 0.75, and 1.0 g/l. Subsequently, 250 ml solutions were prepared under optimal conditions. The data in Fig. 6a indicate that the red hair dye removal decreases as the salt concentration increases. This decline is attributed to competition between sodium ions and pollutant molecules for the available adsorption sites on the adsorbent (Davoudi, 2022; Biuki et al., 2025).

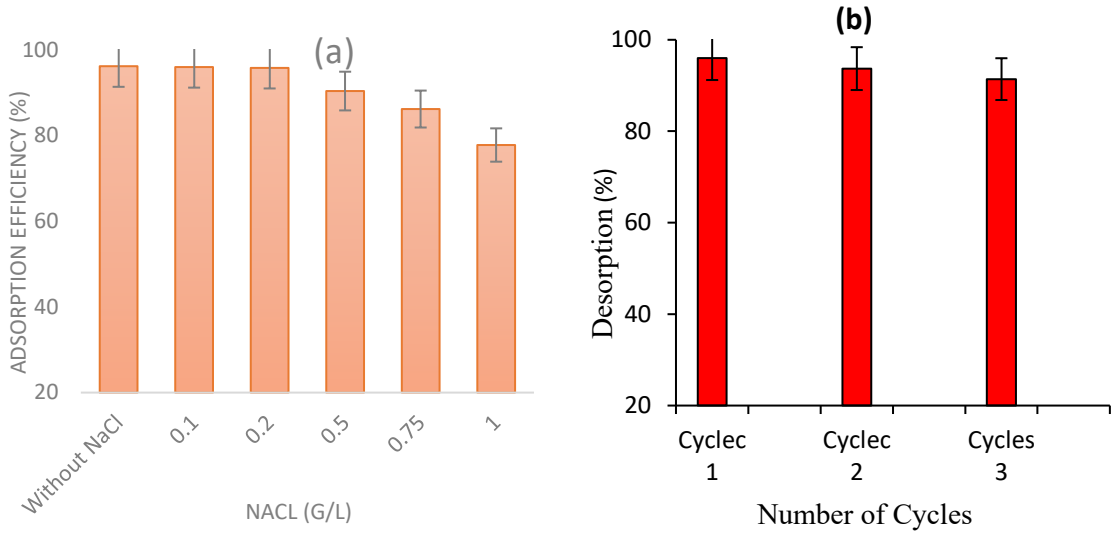

Fig. 6: a) Effect of ionic strength NaCl on the adsorption of red hair dye (pH = 6.5, dosage adsorbent = 0.2 g, t = 65 min), b) Desorption of red hair dye (pH = 6.5, dosage adsorbent = 0.2 g, t = 65 min)

3.9 Desorption of red hair dye and reusability of the adsorbent

In this section, three consecutive adsorption-desorption cycles were carried out using a model ion solution after the material was activated through the adsorption process. The red hair dye recovery rate showed a slight decrease of 2.05% by the third cycle. The first cycle recovered 96.8%, while the second and third cycles yielded 96.4% and 94.8%, respectively. These results indicate that the Fe_3O_4@NH_2-SBA-16NCs adsorbent is reusable, though further cycling is necessary to assess its long-term performance and durability, as shown in (Fig. 6b) (Pournamdari et al., 2024).

3.10 Comparison of adsorption capacity

Many adsorbents have been used to adsorb red hair dye and achievement of wastewater treatment and their operational parameters were compared. This comparison was carried out by the maximum adsorption capacity and maximum adsorption efficiency of various adsorbents in the removal of red hair dye and fuchsin dyes. The results showed the maximum adsorption capacity in this study, although lower than some other adsorbents. But it was higher than some other adsorbents, such (Jamun seed powder biochar, Silybum marianum seed shells, and Polymeric nanocomposite, and respective results are reported in Table 4. The outcomes of the table clearly show that the sorption capacity of the utilized sorbent in the current study is significantly high. In general, morphology, particle size, distribution, and surface structure of this sorbent were effective in its successful outcomes.

Table 4 Studies on the removal of red hair dye and fuchsin dyes by various adsorbents

Dyes	Adsorbent	Dosage adsorbent (g)	pH	Time (min)	Adsorption efficiency (%)	Adsorption capacity (mg/g)	Ref.
Basic fuchsin dye (BF)	Jamun seed powder biochar	0.6	8.0	75	(97.0%)	8.0	Kosale et al., 2023
Basic fuchsin dye (BF)	Polymeric nanocomposite	1.0	6.0	85	(94.1%)	0.43	Kaith et al., 2019
Basic fuchsin dye (BF)	Silybum marianum seed shells (SMSS)	5.0	12.0	60	(97.5%)	7.14	Ali Ahmadi et al., 2024
Basic fuchsin dye (BF)	Walnut shell AC	2.0	8.0	10	(99.1%)	45.45	Biuki et al., 2025
Red hair dye	Oak cupules coated with ZnONPs (COZ)	0.06	7.0	150	(90.5%)	55.5	Al-Ma'abreh et al., 2022
Red hair dye	Fe_3O_4@NH_2-SBA-16NCs	0.2	6.5	65	(96.8 %)	16.1	This work

4. Conclusion

This research considers the synthesis, investigation, and application of Fe_3O_4@NH_2-SBA-16NCs for the removal of red hair dye from aqueous solution. The main findings of this research are:

1. The process of red hair dye removal follows pseudo-second-order kinetics. The Langmuir model provided a better fit of the equilibrium adsorption data. The maximum adsorption capacity q_{max} (16.1 mg/g at 25 °C, respectively).

2.The reusability of the adsorbent for further studies in batch gave rise to encouraging results. The removal efficiency is high of 90% of the synthesized adsorbent.

3- Fe_3O_4@NH_2-SBA-16 NCs adsorbent with chemical structure of consists of silicate sources and Fe_3O_4 nanoparticles, all of which are compatible with the environment, is very inexpensive, energy saving, and most important of all non-toxic.

As a result, it is a promising candidate for wastewater treatment applications, particularly in contexts requiring robust and economical solutions for contaminant remediation.

Statements and Declarations
Data availability

Data will be made available on request**.**

Conflicts of interest

No potential conflict of interest was reported by the author(s).

Author contribution

F. Marahel: Conceptualization of this study, Methodology, writing, review, and editing; H. Neysi: Methodology, writing-original draft; Al. Geramizadegan: Investigation, writing, review, and editing; and S. Shirvan: Investigation, writing-original draft.

AI Use Declaration

During the preparation of this manuscript, the authors used iThenticate and Grammarly. All content has been carefully reviewed and revised by the authors, who take full responsibility for the final version of the manuscript.

References

Abidin, N. H. Z., Ibrahim, W. N. W., Hanapi, N. S. M., Hadzir, N. M., Abdul Karim, S. K., Yahaya, N., & Kamaruzaman, S. (2022). Trace Level Quantification of Organophosphorus Pesticides from Fleshy Fruit Samples by Magnetic Solid-phase Extraction Using Fabricated SBA-15/Fe3O4 Coupled with HPLC/UV. *Analytical and Bioanalytical Chemistry Research. 9* (1), 45-57. https://doi.org/10.22036/ABCR.2021.265794.1578

Ali Ahmed, A., Hattab, Z., Berredjem, Y., Hamoudi, S., & Djellabi, R. (2024). Valorization of Silybum Marianum Seed Shells Waste as Biosorbent for Basic Fuchsin Dye Removal from Water: Kinetics, Isotherms, and Thermodynamic Studies. *Desalination and Water Treatment*. 317, 100278. https://doi.org/10.1016/j.dwt.2024.100278

Ahmad, A., Mohd-Setapar, S. H., Chuo, S. C., Khatoon, A., Wani, W. A., Kumar, R., & Rafatuuah, M. (2015). Recent Advances in New Generation Dye Removal Technologies: Novel. *RSC Advanvces 5*, 3080130818. https://doi.org/10.1039/C4RA16959J

Al-Ma'abreh, A. M., Abuassaf, R. A., Hmedat, D. A., Alkhabbas, M., Edris, G., Hussein-Al-Ali, S. H., & Alawaideh, S. (2022). Adsorption Characteristics of Hair Dyes Removal from Aqueous Solution onto Oak Cupules Powder Coated with ZnO. *International Journal of Molecular Sciences.* 23 (19), 11959. https://doi.org/10.3390/ijms231911959

Anyat, T., Ali, A., Alharati, S., Santali, E. Y., & Iqbal, M. (2025). Facile synthesis of amine functionalized silica coated iron oxide nanoparticles for highly efficient removal of cefixime and ceftriaxone from wastewater. *Separation and Purification Technology, 60* (2), 234-249. https://doi.org/10.1080/01496395.2024.2434536

Biuki, M., Zavvar Mousavi, H., Arvand, M., & Fallah Moafi, H. (2025). Removal of Fuchsin dye from aqueous solutions using walnut shell-derived activated carbon. *Iranian Journal of Chemistry* and *Chemical Engineering* (*IJCCE*). *44*(1), 97-111. https://doi.org/10.30492/IJCCE.2024.2035458.6702

Corrêa, G. T., de Souza, J. C., Pedro Silva, J., Pividori, M. I., & Zanoni, M. V. B. (2020). Determination of temporary dye Basic Red 51 in commercial hair dye, river water and wastewater from hairdressing salon using graphite-epoxy composite electrode modified with magnetic nanoparticles. *Microchemical Journal, 159*, 105485. https://doi.org/10.1016/j.microc.2020.105485

Davoudi, Sh. (2022). Adsorption of Methylene blue (MB) dye Using NiO-SiO_2NPs Synthesized from Aqueous Solutions: Optimization, kinetic and equilibrium studies. *Iranian Journal of Chemistry* and *Chemical Engineering* (*IJCCE*). *41*(7), 2343-2357. https://doi.org/10.30492/IJCCE.2021.526904.4630

Dehvari, M., Ehrampoush, M. H., Ghaneian, M. T., Jamshidi, B., & Tabatabaee, M. (2017). Adsorption Kinetics and Equilibrium Studies of Reactive Red 198 Dye by Cuttlefish Bone Powder. *Iranian Journal of Chemistry* and *Chemical Engineering* (*IJCCE*), *36* (2), 143-151. https://doi.org/10.30492/IJCCE.2017.26703

Einolghozati, Sh., Pournamdari, E., Choobkar, N., & Marahel, F. (2022). Response surface methodology for removal of methyl violet dye using *Albizia stem bark Lebbeck* modified by $Fe_2(MoO_4)_3$ nanocomposite from aqueous solutions and assessment relative error by neural network model. *Desalination and Water Treatment*, *278*, 195-208. https://doi.org/10.5004/dwt.2022.29017

EL–Desouky, M. G., & EL-Bindary, A. A. (2021). Magnetic metal-organic framework (Fe_3O_4@ZIF-8) nanocomposites for adsorption of anionic dyes from wastewater. *Inorganic and Nano-Metal Chemistr-y, 51*, 1-17. https://doi.org/10.1080/24701556.2021.2007131

El Haddad, M. (2016). Removal of basic fuchsin dye from water using mussel shell biomass waste as an adsorbent: equilibrium, kinetics, and thermodynamics. *Journal of Taibah University for Science, 10*(5), 664-674. https://doi.org/10.1016/j.jtusci.2015.08.007

Emrani, Sh., Ebrahimi, M., Zhiani, R., and Motavalizadehkakhky, A. (2023). Removal of Pb (II) from aqueous solutions using magnetic mesoporous silica nanocomposites: modeling and optimization based on response surface methodology. *Journal of Water & Wastewater 33* (6), 67-92. https://doi.org/10.22093/WWJ.2023.379990.3314

Feliczak-Guzik, A., Jadach, B., Piotrowska, H., Murias, M., Lulek, J., & Nowak, I. (2016). Synthesis and characterization of SBA-16 type mesoporous materials containing amine groups. *Microporous and Mesoporous Materials. 220*, 231-238. https://doi.org/10.1016/j.micromeso.2015.09.006

Ghosh, P., & Sinha, A. K. (2008). Hair colors: classification, chemistry and a review of chromatographic and electrophoretic methods for analysis. *Analytical Letters 41*, 2291-2321. https://doi.org/10.1080/00032710802352605

Gupta, V. K., Kumar, R., Nayak, A., Saleh, T. A., & Barakat, M. A. (2013). Adsorptive removal of dyes from aqueous solution onto carbon nanotubes: A review. *Advances in Colloid and Interface Science.* 193-194, 24-34. https://doi.org/10.1016/j.cis.2013.03.003

Jamshidi, K., Ahmad Panahi, H. Sobhan Ardakani, S., & Hassani A.H. (2022). Removal of pyrene from aqueous solutions using GO/Fe_3O_4/CC/AA as a novel adsorbent, *International Journal of Environmenal Analytical Chemistry.* 102 (11), 2625-2640. https://doi.org/10.1080/03067319.2020.1758080

Kaith B.S., Shanker U., & Gupta B. (2019). One-pot green synthesis of polymeric nanocomposite: biodegradation studies and application in sorption degradation of organic pollutants. *Journal of Environmental Management, 234*, 345-356. https://doi.org/10.1016/j.jenvman.2018.12.117

Kiomarsipour, N., Alizadeh, M., Alizadeh, M., and Ghani, K. (2021). Synthesis and surface-functionalizing of ordered mesoporous carbon CMK-3 for removal of nitrate from aqueous solution as an effective adsorbent. *Diamond & Related Materials 116*, 108419. https://doi.org/10.1016/j.diamond.2021.108419

Kosale D., Thakur C., & Singh V. K. (2023). Use of jamun seed (syzyum cumini) biochar for the removal of fuchsin dye from aqueous solution. *Journal of the Serbian Chemical Society, 88* (6), 653-667. https://doi.org/10.2298/JSC220830021K

Li, Y., Sun, J., Du, Q., Zhang, L., Yang, X., Wu, S., Xia, Y., Wang, Z., Xia, L., & Cao, A. (2014). Mechanical and dye adsorption properties of graphene oxide/chitosan composite fibers prepared by wet spinning. *Carbohydrate Polymers 102*, 755-761. https://doi.org/10.1016/j.carbpol.2013.10.094

Marahel, F., Mombeni Goodajdar, B., Niknam, L., Faridnia, M., Pournamdari, E., & Mohammad Doost, S. (2023). Ultrasonic assisted adsorption of methylene blue dye and neural network model for adsorption of methylene blue dye by synthesized Mn-doped PbS nanoparticles. *International Journal of Environmental Analytical Chemistry. 103* (13), 3059-3080. https://doi.org/10.1080/03067319.2021.1901895

Mohamadia, N., Ulay, A., Shahjada, Sh., Enyani, R., & Navarro, A. E. (2023). Comparative biosorption of blue hair dye onto natural polysaccharides. *Environmental Sustainability 6* (1), 73-85. https://doi.org/10.1007/s42398-022-00253-6

Pournamdari, E., & Niknam, L. (2024). Applicability, adsorbent chitosan@ Fe2 (MoO4) 3 nanocomposite for removal of textile reactive red198 dye from wastewater. *Desalination and Water Treatment*. *317*, 100268. https://doi.org/10.1016/j.dwt.2024.100268

Pournamdari, E., Niknam, L., Davoudi, Sh., & Khazali, F. (2024). Response Surface methodology, and artificial neural network model for removal of textile dye reactive yellow 105 from wastewater using zeolitic imidazolate-67 modified by Fe_3O_4 nanoparticles. *International Journal of Phytoremedation.*. *26* (1), 98-113. https://doi.org/10.1080/15226514.2023.2226217

Qin, J., Qiu, F., Rong, X., Yan, J., Zhao, H., & Yang, D. (2014). Removal of basic fuchsin dye from aqueous solutions using graphite oxide modified aromatic polyurethane foam material. *Toxicological and Environmental Chemistry, 96*(6), 849-860. https://doi.org/10.1080/02772248.2014.993642

Radha, F. H. S., Shwan, D. M. S., Kaufhold, S., & Cecilia, J. A. (2023). adsorption study and removal of basic fuchsin dye from medical laboratory wastewater using local natural clay. *Adsorption Science & Technology* 2023 (1), 9398167. https://doi.org/10.1155/2023/9398167

Sobhanardakani, S., Ghoochian, M., Jameh-Bozorghi, S., & Zandipak, R. (2017). Assessing of removal efficiency of indigo carmine from wastewater using MWCNTs. *Iranian Journal of Science and Technology, Transaction A: Science.* 41, 1047-1053. https://doi.org/10.1007/s40995-017-0312-z

Sorour, F. H., Marouf, Y. M., Abd-ElMonem, N.M., Aboeleneen, N. M., & Mansour, R. A. (2024). Raw sawdust utilization for the removal of acid red57 and basic fuchsin dyes from aqueous solution: equilibrium, kinetics, and thermodynamic investigation. *International Journal of Phytoremedation.* 26 (5), 669-683. http://doi.org/10.1080/15226514.2023.2259999

Souza, J. C., Zanoni, M. V. B., & Oliveira-Brett, A. M. (2020). Genotoxic permanent hair dye precursor's p-aminophenol and p-toluenediamine electrochemical oxidation mechanisms and evaluation in biological fluids. *Journal of Electroanalytical Chemistry.* 857, 113509. https://doi.org/10.1016/j.jelechem.2019.113509

Wang, X., Mei, J., Zhao, Z., Chen, Z., Zheng, P., Fu, J., Li, H., Fan, J., Duan, A., & Xu, Ch. (2018). Controllable Synthesis of Spherical Al-SBA-16 mesoporous materials with different crystal sizes and its high isomerization performance for hydrodesulfurization of dibenzothiophene and 4, 6-Dimethyl dibenzothiophene. *Industrial & Engineering Chemistry Research,* 57 (7), 2498-2507. https://doi.org/10.1021/acs.iecr.8b00109

Yang, X., Li, Y., Du, Q., Sun, J., Chen, L., Hu, S., Wang, Z., Xia, Y., & Xia, L. (2015). Highly Effective Removal of Basic Fuchsin from Aqueous Solutions by Anionic Polyacrylamide/Graphene Oxide Aerogels. *Journal* of *Colloid and Interface Science.* 453, 107-114. https://doi.org/10.1016/j.jcis.2015.04.042

Zahir, H., Naidoo, M., Kostadinova, R. M., Ortiz, K. A., Sun-Kou, R., & Navarro, A. E. (2014). Decolorization of hair dye by lignocellulosic waste materials from contaminated waters. *Frontiers in Environmental Science.* 2, 28. https://doi.org/10.3389/fenvs.2014.00028

Zhao, D., Huo, Q., Feng, J., Chmelka, B. F., & Stucky, G.D. (1998). Nonionic Triblock and Star Diblock Copolymer and Oligomeric Surfactant Syntheses of Highly Ordered, Hydrothermally Stable, Mesoporous Silica Structures. *Journal of the American Chemical Society, 120* (24), 6024-6036. https://doi.org/10.1021/ja974025i

Zolfaghari, G., & Zanganeh Assadabadi, A. (2025). Synthesis of Silicate Nanoporous and Its Grafting with Amine and Metal Ligands for the Removal of Cr(VI) in Industry and Environment. *Environment and Water Engineering, 11*(1), 1-10. https://doi.org/10.22034/ewe.2024.441853.1914